Running transverse waves in optical phase conjugation

Jörg Leonardy* and Friedemann Kaiser
Institute of Applied Physics—Nonlinear Dynamics, Technical University of Darmstadt, Hochschulstrasse 4a, 64289 Darmstadt, Germany

Milivoj R. Belić
Institute of Physics, P.O. Box 57, 11001 Belgrade, Yugoslavia
and Department of Physics, Texas A&M University, College Station, Texas 77843-4242

Ortwin Hess
Institute of Technical Physics, Deutsche Forschungsanstalt für Luft- und Raumfahrt e.V., Pfaffenwaldring 38-40, 70569 Stuttgart, Germany

(Received 4 December 1995)

We investigate the dynamics of four-wave mixing processes in photorefractive crystals in paraxial approximation, assuming the phase-conjugation condition. By applying an external electric field to the crystal, we observe an onset of instabilities in the phase-conjugate beam, the generation of running transverse waves, their mutual collisions, and a continuous transition to a regime of spatiotemporal chaos. This state appears as irregularly oscillating defectlike patterns in one transverse dimension. Running transverse waves are identified as the basic modes of the system giving rise to a secondary instability. The observed regular and irregular spatiotemporal oscillations are characterized by means of a spatiotemporal cross-correlation function and singular value decomposition. In the extension to two transverse dimensions the possibility of an even greater variety of regular and irregular patterns is observed. [S1050-2947(96)03206-4]

PACS number(s): 42.65.Sf, 42.65.Hw

I. INTRODUCTION

Transverse and dynamical effects in active and passive optical systems have recently become a topic of increased interest [1]. In addition to displaying a wealth of complex physical phenomena, they represent convenient systems (both theoretically and experimentally) for investigation of possible routes to spatiotemporal chaos. Various scenarios leading to complex spatiotemporal dynamics are often mediated by defects in the transverse amplitude distribution of light beams, hence providing a link to other fields (such as fluid dynamics and condensed matter physics) where defects also play a prominent role in the onset of turbulence.

Photorefractive (PR) oscillators or phase-conjugate (PC) mirrors are essential parts of any envisioned device employing optical phase conjugation (OPC) [2]. Owing to their slow response times, PR oscillators provide an opportunity for a slow-motion study of pattern dynamics, allowing for an observation of complex spatiotemporal pattern formation in real time. This advantage led to the first experimental observation of optical vortices (phase singularities) in a nonlinear optical system, using a unidirectional ring resonator with a PR gain [3]. In the following years there have been many theoretical and experimental studies of spatiotemporal dynamics in unidirectional PR ring resonators [4], bidirectional PR ring resonators [5], and PC resonators with PR crystals acting as PC mirrors [6]. While some phenomena, such as vortex dynamics, periodic alternation, and chaotic itinerancy of cavity modes [7] are well understood, the excitation of running transverse waves (RTW) on the route towards spatiotemporal chaos has not been investigated so far, to the best of our knowledge. Indeed, they should readily be observable in PR optical phase conjugation (OPC), since the necessary ingredients (detuning of PC waves, running gratings, and complex couplings) constitute a part of the normal operation of PR conjugators. We observe RTW in numerical simulations of OPC through the process of four-wave mixing (4WM) in PR crystals. The left- and the right-going RTW appear, collide, and build up localized standing waves in the transverse profiles of the mixing beams. We observe a transition to spatiotemporal chaos associated with oscillating defectlike patterns in the transverse plane. This transition to spatiotemporal chaos is characterized by means of spatiotemporal cross-correlation functions (CCF) and singular value decomposition (SVD).

The paper is composed as follows. Section II presents the transverse model of 4WM in PR crystals in paraxial approximation. The occurrence of RTW and their interactions are discussed in Sec. III. The transition to spatiotemporal chaos is analyzed with the help of CCF (Sec. IV) and SVD (Sec. V). Some results for two transverse dimensions are presented in Sec. VI. Section VII concludes the paper.

II. MODEL EQUATIONS

In the following we will consider the standard photorefractive 4WM processes in transmission geometry [8] (Fig. 1). Basic equations describing the process in paraxial approximation are of the form [9]

$$\partial_z A_1 + \beta \hat{\mathbf{K}} \cdot \nabla_T A_1 + i\phi \nabla_T^2 A_1 = Q A_4, \tag{1a}$$

$$\partial_z A_2 + \beta \hat{\mathbf{K}} \cdot \nabla_T A_2 - i\phi \nabla_T^2 A_2 = Q^* A_3, \tag{1b}$$

$$\partial_z A_3 - \beta \hat{\mathbf{K}} \cdot \nabla_T A_3 - i\phi \nabla_T^2 A_3 = -Q A_2, \tag{1c}$$

*Electronic address: joerg@optics.iap.physik.th-darmstadt.de

 © 1996 The American Physical Society

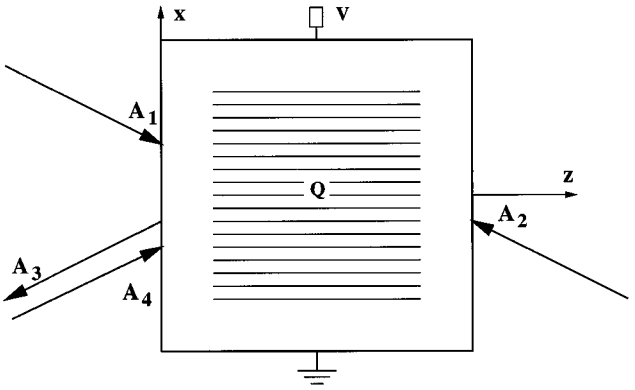

FIG. 1. Geometry of the four-wave mixing process. The pump beams A_1 and A_2 enter the crystal from the opposite side. A_4 is the signal beam and A_3 is the phase-conjugated replica of A_4. z is the propagation direction and x is one of the transverse directions, the other, y, being perpendicular to the x-z plane. Q represents the amplitude of the transmission grating and V is the high-voltage source of the static electric field E_0.

$$\partial_z A_4 - \beta\hat{\mathbf{K}}\cdot\nabla_T A_4 + i\phi\nabla_T^2 A_4 = -Q^* A_1, \tag{1d}$$

where $A_j(x,y,z)$ are the slowly varying envelopes of the four beams, ∇_T^2 is the transverse Laplacian, and ϕ is a measure for the magnitude of diffraction. The operator $\hat{\mathbf{K}}\cdot\nabla_T$ is the directional derivative in the transverse plane along the grating wave vector $\hat{\mathbf{K}}$, and β is the relative transverse displacement caused by the noncollinear propagation of the four beams. In scaled coordinates $\beta=\theta/\delta$, where θ is the half angle at the beam intersection and δ is the angular spread of the interacting beams. Q is the complex amplitude of the transmission grating in the crystal, whose temporal evolution is approximated by a relaxation equation of the form [10]

$$\tau\partial_t Q + \frac{E_D+E_q+iE_0}{E_M+E_D+iE_0}Q = \frac{\gamma_0}{I_0}\frac{E_q+E_D}{E_D}\frac{E_D+iE_0}{E_M+E_D+iE_0}(A_1A_4^*+A_2^*A_3), \tag{2}$$

where τ is the relaxation time constant of the grating, I_0 is the total light intensity, and γ_0 is the bare PR coupling constant. E_D, E_q, and E_M are the characteristic internal fields describing the electronic processes in the crystal (according to Kukhtarev *et al.* [10]), whereas E_0 is the static external electrical field applied to the crystal. Note that E_0 effectively renders both the coupling constant γ_0 and the relaxation rate (τ^{-1}) complex. Hence the external field E_0 exerts a profound influence on the process of OPC, e.g., by breaking the frequency degeneracy, allowing for the buildup of running gratings and the appearance of RTW. Note further that in writing Eq. (2), we assume that the wave number of the grating $\hat{\mathbf{K}}$ is small compared to the Debye screening wave number k_D [11]. Consequently, the implicit assumption of neglecting the transverse derivatives of Q is well justified.

Equations (1) and (2) are solved numerically using the beam propagation method described in [9]. An alternative Crank-Nicholson procedure is employed in unstable situations, to eliminate the possibility of looking at numerical rather than physical instabilities. Results obtained by both methods are in excellent agreement. Boundary conditions play an important role in every investigation of RTW and vortex dynamics. In fact, some of the results on pattern formation due to the occurrence of traveling waves reported elsewhere [12] are obtained only by assuming rather special boundary conditions. Here the boundary conditions are chosen consistently with the corresponding experimental conditions. Displaced Gaussian beams are chosen for incident fields at the opposite faces of the crystal, in combination with ''open'' lateral sides (no reflecting or periodic boundary conditions). Transverse patterns appear spontaneously. To prevent aliasing and overshooting problems, the fields A_j are smoothly damped at the edge of the transverse numerical grid. Thus far, the input beams are given by

$$A_{4,1}(x,z=0)=C_{4,1}G(-\zeta,\rho), \quad A_{2,3}(x,z=d)=C_{2,3}G(\zeta,\rho), \tag{3}$$

where C_{1-4} are the amplitudes of the Gaussian beams incident upon the crystal and $G(\zeta,\rho)$ is the Gaussian beam function [9]. ζ represents the beam curvature parameter and $\rho^2=(x\pm\beta/2)^2+(y\pm\beta/2)^2$.

The parameters used in the simulations are chosen as follows. The longitudinal coordinate (z) is normalized to the crystal length d and the transverse coordinates (x,y) are normalized to the beam diameter. $E_M=100$, $E_q=5$, $E_D=1$ (given in kV/cm), $\gamma_0 d=-4$, and $\phi=0.0005$. The amplitudes of the input beams are $C_1=0.3$, $C_2=0.7$, and $C_4=0.15$, whereas C_3 is chosen to be small (in our simulations 10^{-9}, just enough to provide a seed for the PC beam). Practically, a PC condition is assumed. With such a set of parameters, and in particular without applying an external electric field (i.e., $E_0=0$), we do not observe instabilities of any kind.

III. RUNNING TRANSVERSE WAVES AND THEIR INTERACTION

The application of an external electrical field E_0 across the PR crystal changes the dynamical behavior of the PC process. Normally, an external field is applied to restore a $\pi/2$ phase shift between the interference fringes and the refractive index gratings, enhancing the process of phase conjugation. In our case, the situation is reversed. Starting with a degenerate oscillation and a $\pi/2$ shift, we apply the field E_0 to produce frequency detuning, and to study the destabilization of the PC process. As the electric field is increased, we observe the appearance of basic RTW, their collision, and complicated dynamics resulting from their interactions, leading to spatiotemporal chaos. Note that chaos in the temporal regime on the basis of a plane-wave model has already been investigated [13]. However, we concentrate on the combined influence of spatial and temporal effects.

Figure 2 displays the basic right-going and left-going RTW. The spatiotemporal dynamics of the PC intensity $I_3(x,z=0)\equiv I_{30}$ is shown for the value of $E_0=1.8$ kV/cm and for $\beta=\pm 0.05$, in one transverse dimension. Sources of waves are located at the left transverse edge for the right-going RTW, and at the right transverse edge for the left-going RTW. The RTW travels transversally towards the beam center and is absorbed in a sink at the opposite transverse edge.

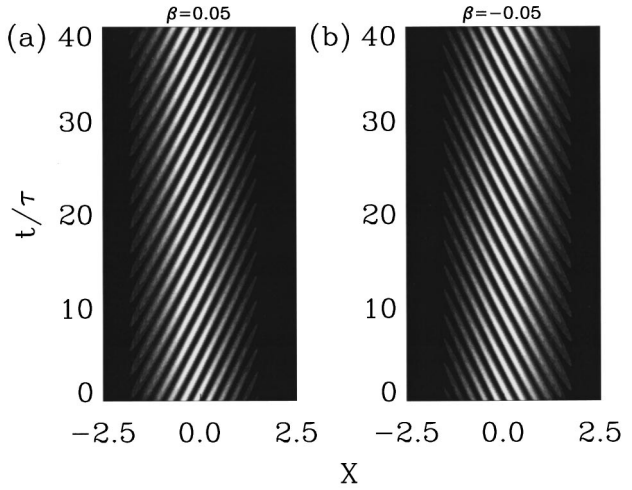

FIG. 2. Spatiotemporal dynamics of $I_3(x,z=0)\equiv I_{30}$ as measured at the surface of the crystal at $z=0$. Bright regions represent high light intensity, dark regions indicates low intensity. (a) Right-going RTW with $\beta=0.05$. (b) Left-going RTW with $\beta=-0.05$. $E_0=1.8$ kV/cm. In all figures the transverse coordinates (x,y) are normalized to the beam diameter.

Reduction in the value of β leads to the combined appearance of both left-going and right-going RTW. For sufficiently small values of β the initial conditions (and not the sign of β) determine the appearance of left-going and right-going RTW. For $\beta=0.001$ and for low values of E_0 (up to $E_0\approx 1.2$ kV/cm), a stable oscillation (fixed point) with Gaussian transverse profiles for the four beams is found. At $E_0=1.21$ kV/cm this stable oscillation loses stability (Fig. 3), and a ''fish-bone'' instability arises, in which a left-going and a right-going RTW collide. In this case sources are located at both transverse edges and the sink of the RTW appears as a localized standing wave in the center of the beam.

In order to provide direct information on the spatiotemporal dynamics of RTW, we plot the transverse intensity and phase of the right-going RTW and the ''fish-bone'' oscillation (Fig. 4). The tilt of the phase ϕ_3 of the beam I_3 indicates the size and the direction of the transverse wave vector k_x of

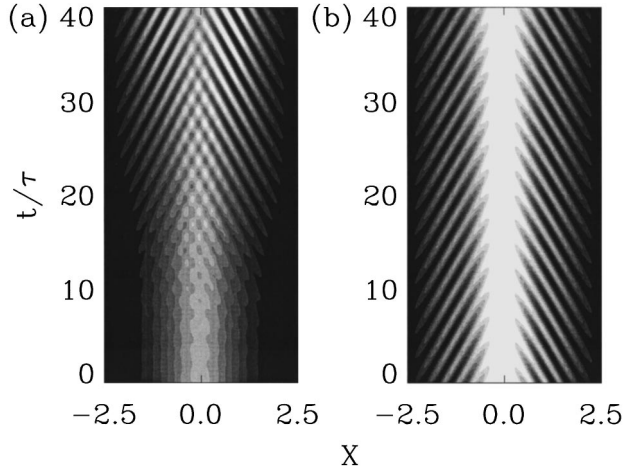

FIG. 3. Spatiotemporal dynamics of I_{30} with $\beta=0.001$ and $E_0=1.21$ kV/cm. (a) Onset of the spatiotemporal oscillation, (b) ''fish-bone'' oscillation after transients have died away.

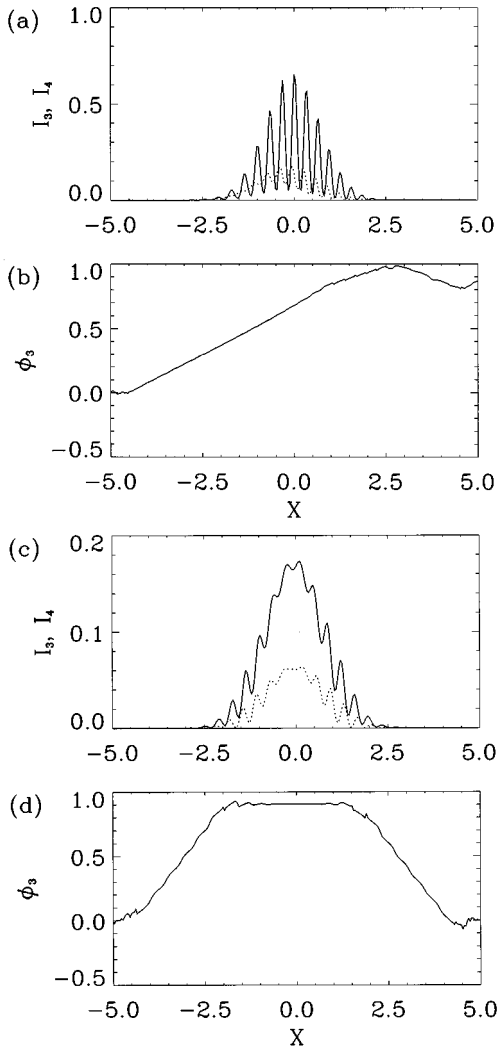

FIG. 4. Transverse intensity and phase profiles in the middle of the PR crystal $(z=d/2)$. (a) Intensity of the right-going RTW with the parameters of Fig. 2(a). (c) Intensity of the ''fish-bone'' oscillation (parameters as in Fig. 3). The dashed lines are the corresponding intensity profiles of I_4 at $z=d/2$. The corresponding phase profiles ϕ_3 at $z=d/2$ of the right-going RTW (b) and the ''fish-bone'' oscillation (d) are also shown. The intensity is given in units of the sum of the incident pump intensitites (C_1+C_2).

RTW. Figure 4(d) of the ''fish-bone'' oscillation depicts the collision of the right-going and the left-going RTW, and the resulting standing-wave pattern in the middle where the phase profile is flat.

An increase in E_0 leads to an increase in the amplitude of the left-going RTW, and a decrease in the amplitude of the right-going RTW (Fig. 5). Consequently, the resulting standing wave is shifted away from the center of the beam. The inverted symmetric oscillation with respect to the center $(x=0)$ axis can be stabilized by changing the initial condition for Q. For values of E_0 beyond 2.0 kV/cm both periodic oscillations lose their stability. A regime of irregular oscillations is established for $E_0=2.2$ kV/cm, and the state of spatiotemporal chaos is reached for $E_0=2.3$ kV/cm. This state is characterized by chaotic wandering of a defectlike structure (line defect), located where the modulated left-going and right-going wave collide. Similar scenarios are observed in

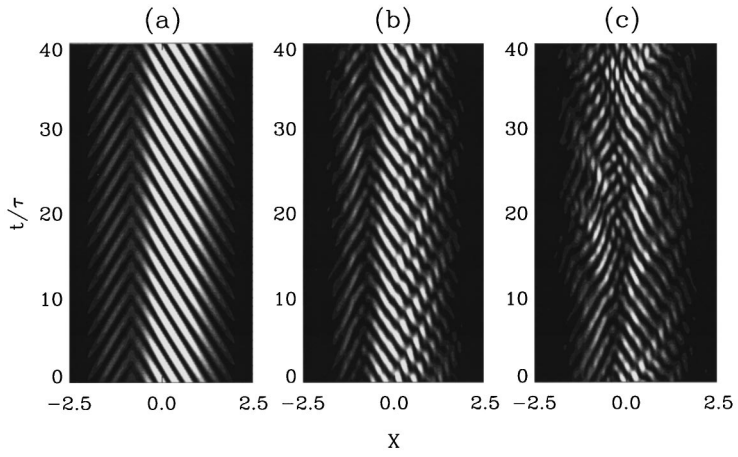

FIG. 5. Spatiotemporal dynamics of I_{30} with $\beta=0.001$ and (a) $E_0=1.35$, (b) $E_0=2.2$, and (c) $E_0=2.3$ (E_0 given in kV/cm).

the solution of the one-dimensional complex Ginzburg-Landau equation [14] as well as in fluid wave patterns [15].

IV. SPATIOTEMPORAL CORRELATIONS

The calculation of correlation functions facilitates the understanding of complex spatiotemporal dynamics [16]. We calculate the cross-correlation function (CCF), defined as

$$C(x_0,\eta)=\frac{\langle \delta I(x_c+x_0,t')\,\delta I(x_c-x_0,t'+\eta)\rangle_T}{\sqrt{\langle \delta I^2(x_c+x_0,t')\rangle_T}\sqrt{\langle \delta I^2(x_c-x_0,t')\rangle_T}}, \tag{4}$$

where $\langle\cdots\rangle_T$ is the average over the whole observation time T, and $\delta I(x,t')=I(x,t')-\langle I(x,t')\rangle_T$ is the intensity deviation at the point x. Thus, the correlation function determines how much the output signal at the reference point x_c+x_0 and at the time $t'=t/\tau$ is correlated to the signal at the transverse position x_c-x_0 and at the time $t'+\eta$. x_c represents the spatial reference point.

The spatiotemporal dynamics of I_{30} is considered for a period of $t=400\tau$ intervals after transients have ''died away.'' We assume this to be representative of its long-time behavior. Figure 6 displays contour plots of the spatiotemporal CCF C. Dark regions indicate anticorrelation, bright regions indicate high correlation. The reference point x_c is placed in the center of the beam at the exit face of the crystal ($x_c=-\beta/2$ for I_{30}). CCF of the basic RTW (not shown here) is a direct image of the original pattern, displaying periodically oscillating and spatially tilted stripes of high correlation (indicating propagation of RTW). CCF of the ''fish-bone'' oscillation [Fig. 6(a)] is periodic in time. A spatial correlation length cannot be identified, indicating that the left-going RTW and the right-going RTW are decoupled in space. Two different regions can be identified in the correlation function of the periodic oscillation state at $E_0=1.35$ kV/cm [Fig. 6(b)]. In the central region ($0\leqslant x_0\leqslant 0.75$) tilted stripes indicate that the left-going RTW is dominant. Here a nonzero correlation length is found, while the typical correlation time is the same as for the ''fish-bone'' oscillation. In the spatially decoupled region ($x_0\geqslant 0.75$), the spatiotemporal evolution of C is similar to the one seen in the case of the ''fish-bone'' oscillation, indicating the presence of both left-going and right-going RTW. CCF pertaining to the irregular oscillating state at $E_0=$ 2.2 kV/cm shows a slight decrease of the high correlation stripes, whereas a rapid decrease of the correlation function is observed for $x_0\geqslant 0.75$ [Fig. 6(c)]. Finally, in the spatiotemporal chaos, a rapid decrease of C in space and time is observed [Fig. 6(d)].

To highlight the role and define a measure for the transverse complexity, we determine the maxima of C with respect to all delay times η,

$$C_{max}(x_0)=\max_\eta C(x_0,\eta). \tag{5}$$

C_{max} thus represents a measure of transverse correlations. Plotting C_{max} versus the transverse distance x_0 allows for a quantitative comparison of different spatiotemporal states

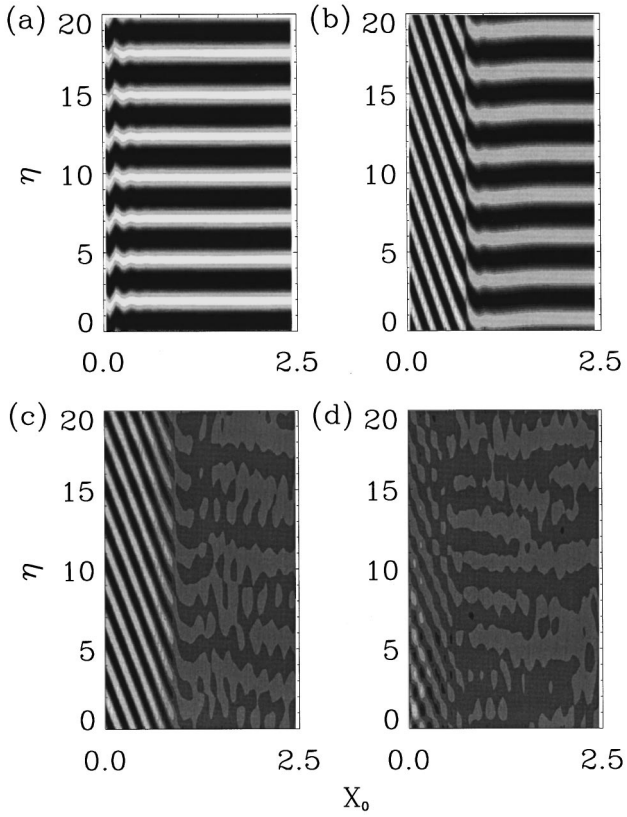

FIG. 6. Gray scale plots of the spatiotemporal cross-correlation function $C(x_0,\eta)$ of I_{30} versus the spatial reference point x_0 and the delay time η. (a) The ''fish-bone'' oscillation of Fig. 3(b). (b)–(d) The periodic and chaotic oscillations of Fig. 5, respectively.

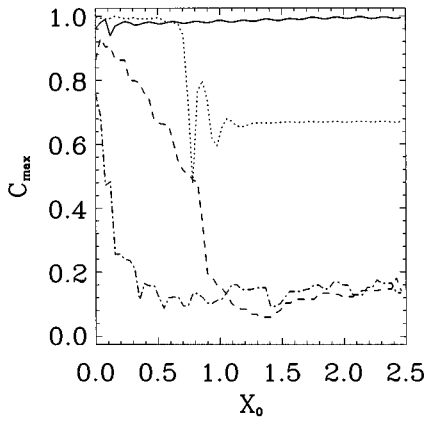

FIG. 7. Temporal maxima C_{max} of the spatiotemporal cross-correlation function versus the transverse distance x_0 extracted from the data of Fig. 6: $E_0=1.21$ (solid line), $E_0=1.35$ (dotted), $E_0=2.2$ (dashed), and $E_0=2.3$ (chain-dotted) (E_0 given in kV/cm).

(Fig. 7). C_{max} pertaining to the RTW and the ''fish-bone'' oscillation is constant and/or slightly oscillating below $C_{max}=1$, indicating spatiotemporally ordered states. In the C_{max} corresponding to the periodic oscillation at $E_0=1.35$ kV/cm, we can recognize the two different regions mentioned above. Note that C_{max} in the decoupled region is much smaller than C_{max} in the center region. For the irregular oscillating state we observe a decrease of C_{max} with increasing x_0, and for the final spatiotemporal chaotic state we observe an exponential decay, which indicates the presence of spatiotemporal chaos [3,17].

V. DYNAMICS OF COHERENT STRUCTURES

In order to quantitatively characterize the large variety of different spatiotemporal oscillations noticed in our 4WM simulations, we apply the singular value decomposition (SVD) or the Karhunen-Loève decomposition [18]. SVD has proven a powerful tool in determining and distinguishing different spatiotemporal degrees of freedom, which are most often hard to detect by visual inspection [18,19]. By computing and analyzing the basic eigenmodes, we obtain a better

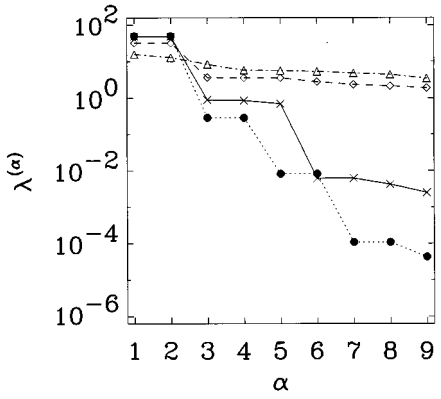

FIG. 8. Spectra of the normalized eigenvalues $\lambda^{(\alpha)}$ calculated from the data of I_{30}: filled dots, RTW [Fig. 2(a)]; crosses, ''fish-bone'' oscillation [Fig. 3(b)]; rhombuses, irregular oscillation [Fig. 5(b)]; triangles, spatiotemporal chaotic state [Fig. 5(c)].

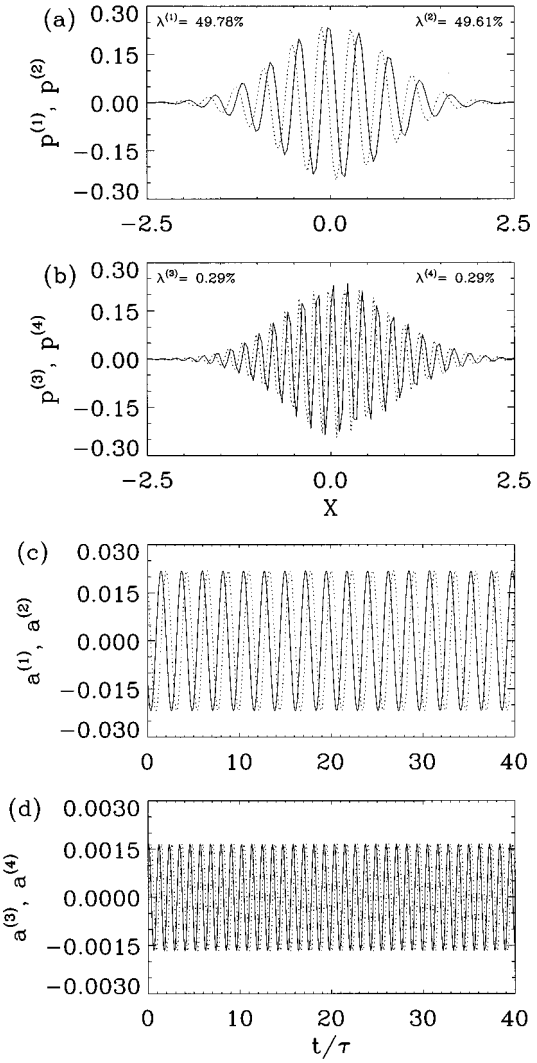

FIG. 9. Eigenmodes of the intensity I_{30} of the RTW of Fig. 2(a). (a) The first (largest) eigenmode (solid line) $\mathbf{p}^{(1)}(x)$ and the second eigenmode (dashed) $\mathbf{p}^{(2)}(x)$. (b) The third eigenmode (solid line) $\mathbf{p}^{(3)}(x)$ and the fourth eigenmode (dashed) $\mathbf{p}^{(4)}(x)$. The superscripts denote the respective eigenvalues $\lambda^{(\alpha)}$. (c) Time dependence of the expansion coefficients $a^{(1)}$ (solid line) and $a^{(2)}$ (dashed). (d) Time dependence of the expansion coefficients $a^{(3)}$ (solid line) and $a^{(4)}$(dashed).

insight into the mechanisms leading to complex and chaotic spatiotemporal dynamics.

The procedure for the SVD starts with the calculation of the spatial covariance matrix of the transversally discretized intensity distribution

$$C_{k,l}=\langle u(x_k,t')u(x_l,t')\rangle_T, \tag{6}$$

where $k,l=1,2,\ldots,N$ is the number of the discrete transverse points x_k and $u(x_k,t)$ is the intensity fluctuation $u(x,t)=\delta I(x,t)/\sqrt{\langle I(x,t)\rangle_T}$, where δI is defined in the preceding section. Eigenvectors $\mathbf{p}^{(\alpha)}$ of $C_{k,l}$ represent an optimal basis for expansion of $I(x,t)$. They maximize the projected mean $\langle(\mathbf{p},u)^2\rangle_T$, where $(\mathbf{p},u)=\Sigma_k\mathbf{p}(x_k)u(x_k,t)$ denotes the scalar product, i.e., the eigenvectors provide a minimum number of eigenmodes needed in the expansion. By construction, $C_{k,l}$ is symmetric and its eigenvalues $\lambda^{(\alpha)}$

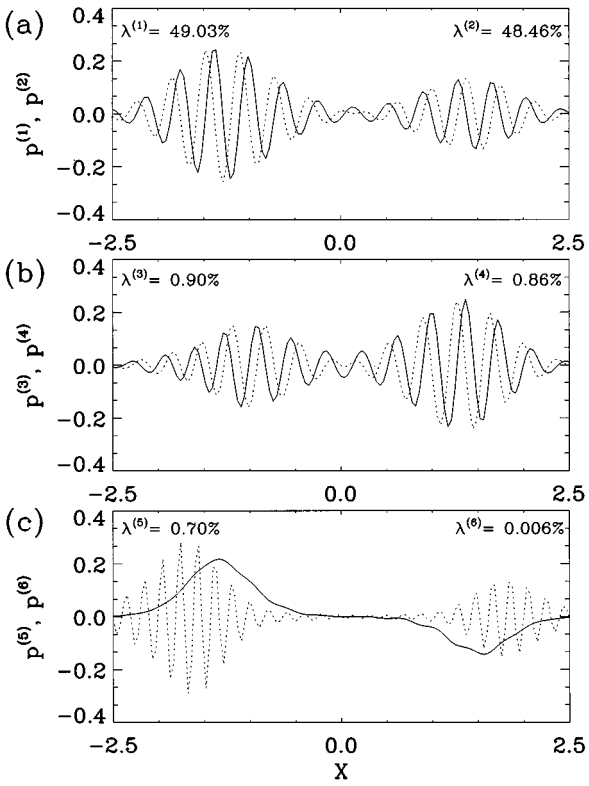

FIG. 10. Eigenmodes of the intensity I_{30} of the ''fish-bone'' oscillation of Fig. 3(b). (a) $\mathbf{p}^{(1)}(x)$ (solid), $\mathbf{p}^{(2)}(x)$ (dashed). (b) $\mathbf{p}^{(3)}(x)$ (solid), $\mathbf{p}^{(4)}(x)$ (dashed). (c) $\mathbf{p}^{(5)}(x)$ (solid) and $\mathbf{p}^{(6)}(x)$ (dashed).

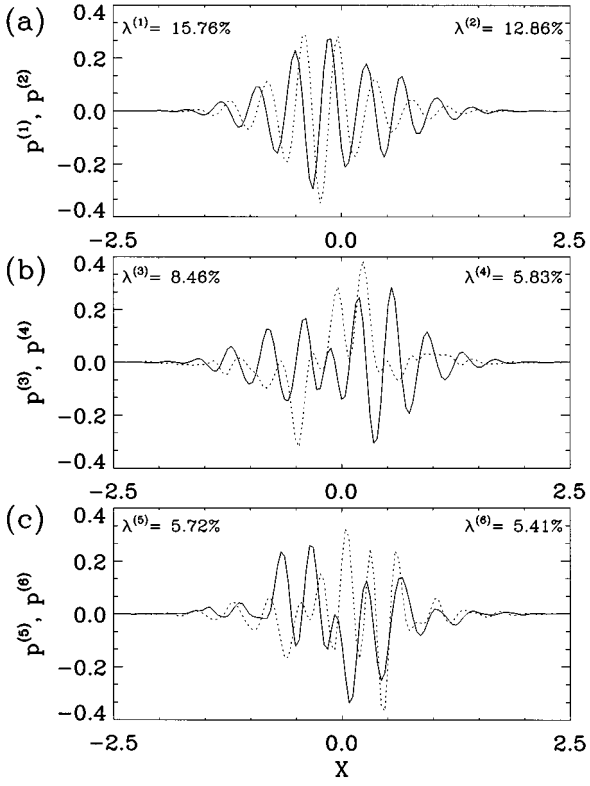

FIG. 11. Eigenmodes of the intensity I_{30} of the spatiotemporal chaotic state of Fig. 5(c). (a) $\mathbf{p}^{(1)}(x)$ (solid), $\mathbf{p}^{(2)}(x)$ (dashed). (b) $\mathbf{p}^{(3)}(x)$ (solid), $\mathbf{p}^{(4)}(x)$ (dashed). (c) $\mathbf{p}^{(5)}(x)$ (solid) and $\mathbf{p}^{(6)}(x)$ (dashed).

determine the probability of the occurrence of the corresponding eigenvectors $\mathbf{p}^{\alpha}$ in the intensity field $u(x,t)$. In the following, the eigenvalues are normalized by $\langle (u,u)\rangle_T = \Sigma_{\alpha=1}^{M} \lambda^{(\alpha)}$. The N eigenvectors $\mathbf{p}^{(\alpha)}(x_k)$ form a complete orthonormal set $\Sigma_k \mathbf{p}^{(\alpha)}(x_k)\mathbf{p}^{(\beta)}(x_k) = \delta^{\alpha\beta}$ and are used as basis functions for an expansion of the original intensity distribution [19]:

$$\delta I(x_k,t) = I(x_k,t) - \langle I(x_k,t)\rangle_T = \sum_{\alpha} a^{(\alpha)}(t)\mathbf{p}^{(\alpha)}(x_k), \tag{7}$$

where the time dependent expansion coefficients are given by

$$a^{(\alpha)}(t) = \sum_{k} \mathbf{p}^{(\alpha)}(x_k)\,\delta I(x_k,t). \tag{8}$$

Figure 8 exhibits the spectrum of the normalized eigenvalues $\lambda^{(\alpha)}$, for the dynamic states considered thus far, the RTW, the ''fish-bone'' oscillation, the irregular oscillation, and the spatiotemporal chaotic state. For the RTW and the ''fish-bone'' oscillation the eigenvalues decrease rapidly with increasing α. The two largest eigenmodes contain more than 97% of the original spatiotemporal information. Note that the eigenvalues of RTW are arranged in pairs. Eigenmode spectra of the chaotic states indicate that the number of modes needed for a reconstruction of the original oscillation increases, pointing to an increase in the number of intrinsically excited degrees of freedom. The information on the spatiotemporal complexity of the dynamic states considered thus far, provided by SVD, agrees well with the results obtained by analyzing the spatiotemporal correlations of those states.

In Fig. 9 the transverse dependence of the four largest eigenmodes and time-series of the corresponding expansion coefficients of the RTW is shown. Both $\mathbf{p}^{(1)}$ and $\mathbf{p}^{(2)}$ repre-

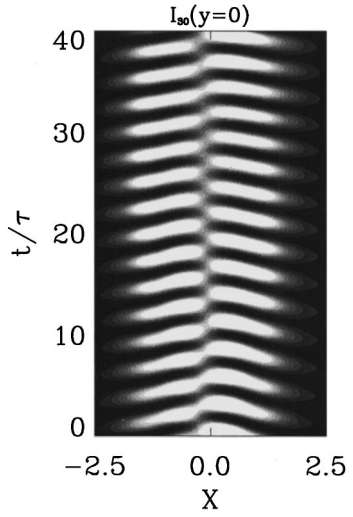

FIG. 12. Spatiotemporal dynamics of I_{30} after transients have died away. The two-dimensional plane is cut at $y=0$, $\beta=0.05$, $\phi=0.01$, and $E_0=1.5$ kV/cm. The other parameters are the same as in the case of one transverse dimension.

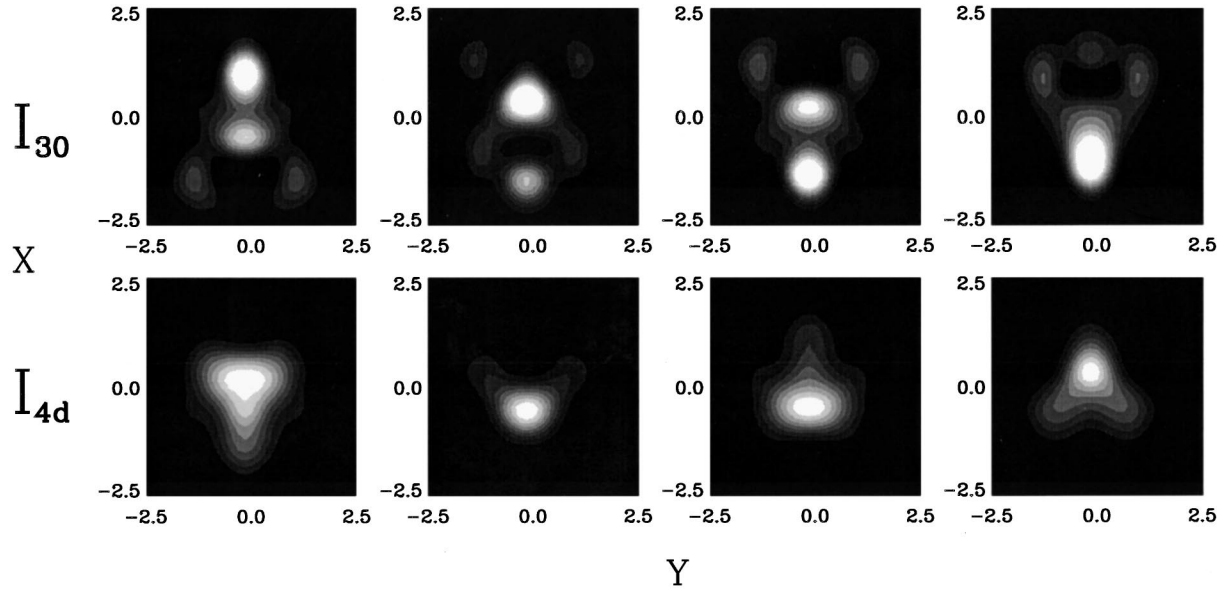

FIG. 13. Two-dimensional transverse pattern of I_{30} and I_{4d} (same parameters as in Fig. 12). The patterns to the left are recorded at $t=21.6\tau$. From left to right, the time interval between the successive patterns is 0.4τ.

sent a transverse standing wave, with a relative phase shift of $\pi/2$. The corresponding expansion coefficients also show a relative phase shift of $\pi/2$, indicating the propagation of RTW. The third and the fourth eigenmode have both spatially and temporally the structure of higher harmonic oscillations with respect to the two largest eigenmodes, and provide very weak corrections to the original.

For the dynamic state where we observe the ''fish-bone'' oscillation, the results obtained by applying the SVD analysis are more diverse (Fig. 10) than in the case of RTW. The transverse dependence of the two largest eigenmodes clearly displays the collision of the left-going and the right-going RTW. This indicates the appearance of both left-going and right-going RTW. The third and the fourth eigenmode are pairwise antisymmetric with respect to $\mathbf{p}^{(1)}$ and $\mathbf{p}^{(2)}$, and lead to corrections in the dominating pattern, given by $\mathbf{p}^{(1)}$ and $\mathbf{p}^{(2)}$. It is interesting to note that in the coexisting spatially reflected symmetric oscillation, which can be stabilized by changing the initial conditions, the third and fourth eigenmode are dominant, while the first and the second eigenmode provide slight corrections to the original. Additionally, the fifth eigenmode represents the symmetry breaking mode, which is visible in the original pattern (cf. Fig. 3). It shifts the pattern to one side.

For the state of spatiotemporal chaos, Fig. 11 shows the transverse dependence of the six largest eigenmodes. The transverse dependence of the eigenmodes reflects the presence of a number of different modulated standing wave patterns which have all the same spatial frequency. However, the ''basic'' standing wave pattern of the RTW, represented by $\mathbf{p}^{(1)}$ and $\mathbf{p}^{(2)}$, is still present in the spatiotemporal chaotic pattern. In time, those eigenmodes show chaotic oscillations.

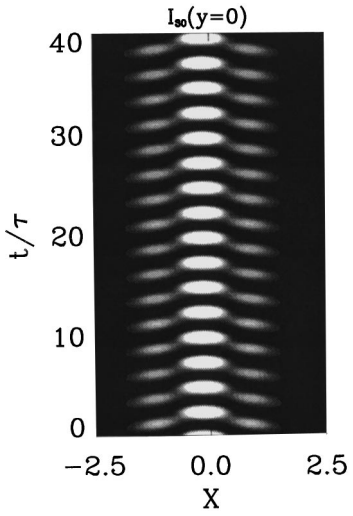

FIG. 14. Spatiotemporal dynamics of I_{30} after transients have died away. The two-dimensional plane is cut at $y=0$. Here, $\beta=0.0001$, $\phi=0.01$, and $E_0=1.8$ kV/cm. The other parameters are the same as in the case of one transverse dimension.

VI. TWO TRANSVERSE DIMENSIONS

Thus far we have been considering the problem of RTW and the excitation of complicated spatiotemporal dynamics with one transverse spatial dimension. In the following, we extend our discussion to the case of two transverse dimensions. With an additional spatial degree of freedom, one might expect the appearance of RTW and other transverse patterns to be more diverse. In our two-dimensional simulations we choose the following geometry. The grating wave vector $\hat{\mathbf{K}}$ points along the x axis and the mixing beams are displaced in the x-z–plane, i.e., $\beta=\beta_x$ and $\beta_y=0$. Here, we restrict our discussion to $I_3(x,y,z=0)\equiv I_{30}$ and $I_4(x,y,z=d)\equiv I_{4d}$.

For $\beta=0.05$ and for small values of E_0 (up to $E_0\approx$ 1.4 kV/cm), only stationary states (fixed points) are found. These states appear as temporally constant values for the four beams with Gaussian profiles (the center of the Gaussian is placed at $x=-\beta/2$ and $y=0$ for I_{30}). At $E_0=1.5$ kV/cm we

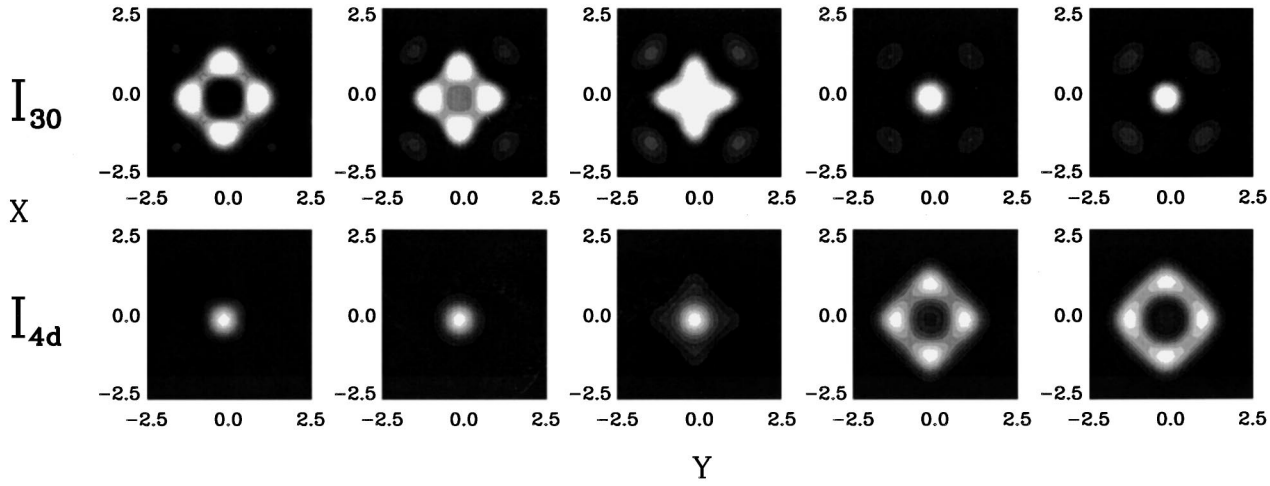

FIG. 15. Two-dimensional transverse pattern of I_{30} and I_{4d} (same parameters as in Fig. 14). The patterns are taken at $t=11\tau$, $t=11.4\tau$, $t=11.6\tau$, $t=12\tau$, and $t=12.4\tau$, respectively.

observe the onset of spatiotemporal oscillations. Figure 12 presents periodic spatiotemporal dynamics of I_{30}, where the transverse plane x-y is cut along the $y=0$ axis. The basic structure, similar in appearance to the left-going RTW and right-going RTW of the one-dimensional transverse case, is visible. However, the waves do not collide and do not form standing wave patterns in the middle as seen in the ''fish-bone'' oscillation. The reason for this difference can be deduced from a direct visualization of the two-dimensional intensity patterns in the spatial dependence of I_{30} (Fig. 13). We observe the following dynamical behavior. Initially, a bright spot is generated off-the-center, it moves towards the center, in whose vicinity it is absorbed. Subsequently, a bright spot arises at the opposite side, executing the same kind of motion. A similar arrangement of periodic oscillating spots distributed along one transverse direction has recently been observed in a self-pumped phase conjugator [20]. Note that the patterns of I_{4d} are partially anticorrelated with the corresponding patterns of I_{30}.

When β is reduced to $\beta=0.001$, an increase of E_0 leads to complicated spatiotemporal dynamics. This is clearly visible in Fig. 14, where the temporal evolution of I_3 at $E_0=1.8$ kV/cm is illustrated. Here a bright spot in the center oscillates in alternation with two spots of lower intensity located at both sides of it. The sequence of corresponding two-dimensional spatial patterns of I_{30} and I_{4d} are plotted in Fig. 15. The dynamic evolution of I_{30} represents a periodic oscillation between two different modelike structures, with different spatial symmetries. This kind of periodic alternation was also observed experimentally in a unidirectional PR ring resonator [7]. Further increase of E_0 leads to increased complexity of the spatiotemporal dynamics, however as long as β is sufficiently small, the inversion symmetry of the patterns is conserved. Here the patterns are similar to the phase-singularity crystals discussed in laser systems [21]. With β increased, we observe complicated dynamics pertaining to symmetry broken patterns.

We should mention that, although work has been started concerning spatiotemporal chaos in two transverse dimensions, progress is slow, owing to high computational demands and costs. Work in that direction has been started.

VII. CONCLUSIONS

In summary, we have demonstrated the appearance of running transverse waves in a model of optical phase conjugation through the process of photorefractive four-wave mixing. Our model includes diffraction, as well as noncollinear propagation of the mixing beams. We have shown that the presence of an external static electrical field (which causes a phase shift in the coupling and a shift of the optical frequency of the PC wave) leads to complicated spatiotemporal oscillations, when transverse dimensions are taken into account. Further, an increase in E_0 leads to a regime of irregular oscillations. This state displays spatiotemporal chaos resembling chaotic wandering of defectlike structures (line defects).

To characterize the observed spatiotemporal dynamics, we employ two different nonlinear dynamical methods, the spatiotemporal cross-correlation function and the singular value decomposition. They provide mutually consistent information when applied to our data. We have shown that the cross-correlation function decreases rapidly in space and time with increasing values of E_0. At the same time, the number of relevant eigenmodes obtained by SVD (which is related to the intrinsic degrees of freedom) increases with increasing E_0. SVD turned out to be a convenient tool not only for the quantification of spatiotemporal complexity, but also for the identification of the dominant nonlinear eigenmodes of the interacting beams. RTW is described by two basic eigenmodes, which oscillate regularly in time. These basic eigenmodes are essential elements in all presented periodic spatiotemporal oscillations, especially for the states where two RTW collide. They also appear and persist as the most dominant eigenmodes in the spatiotemporal chaotic regime. Thus, the RTW is a basic element of the spatiotemporal dynamics during the process of 4WM.

Finally, the appearance of RTW in two transverse dimensions has also been observed. Here, the left-going and right-going RTW appear as two bright spots generated off-the-center, moving alternatingly towards the center in whose vicinity they get absorbed. We observe further periodic alternation between different modelike structures, as well as inversion symmetric patterns, similar to phase-singularity crystals. Such spatiotemporal phenomena are under current investigation.

ACKNOWLEDGMENTS

Work at the Institute of Applied Physics, TH Darmstadt is financially supported within the Sonderforschungsbereich 185 ''Nichtlineare Dynamik'' of the Deutsche Forschungsgemeinschaft. Work at the Department of Physics, Texas A&M University is in part supported by National Science Foundation Grant No. DMR 9215231. J.L. would like to thank Markus Münkel for valuable and interesting discussions.

[1] N. B. Abraham and W. J. Firth, J. Opt. Soc. Am. B **7**, 951 (1990); L. A. Lugiato, Chaos, Solitons & Fractals **4**, 1251 (1994), and numerous references cited therein.

[2] B. Fischer, S. Sternklar, and S. Weiss, IEEE J. Quantum Electron. **QE-25**, 550 (1989).

[3] F. T. Arecchi, G. Giacomelli, P. L. Ramazza, and S. Residori, Phys. Rev. Lett. **67**, 3749 (1991); F. T. Arecchi, Physica D **51**, 450 (1991).

[4] G. D'Alessandro, Phys. Rev. A **46**, 2791 (1992); D. Hennequin, L. Dambly, D. Dangoisse, and P. Glorieux, J. Opt. Soc. Am. B **11**, 676 (1994); B. M. Jost and B. E. A. Saleh, Phys. Rev. A **51**, 1539 (1995).

[5] Z. Chen and N. B. Abraham, Appl. Phys. B **60**, S183 (1995); Z. Chen, D. McGee, and N. B. Abraham (unpublished).

[6] S. R. Liu and G. Indebetouw, J. Opt. Soc. Am. B **9**, 1507 (1992); S. R. Liu and G. Indebetouw, Opt. Commun. **101**, 442 (1993); G. Balzer, S. Matamontero, M. Vasnetsov, and T. Tschudi, J. Mod. Opt. **41**, 807 (1994); D. R. Korwan and G. Indebetouw, Opt. Commun. **119**, 305 (1995).

[7] F. T. Arecchi, G. Giacomelli, P. L. Ramazza, and S. Residori, Phys. Rev. Lett. **65**, 2531 (1990).

[8] M. Cronin-Golomb, B. Fischer, J. O. White, and A. Yariv, IEEE J. Quantum Electron. **QE-20**, 12 (1984).

[9] M. R. Belić, J. Leonardy, D. Timotijević, and F. Kaiser, Opt. Commun. **111**, 99 (1994); J. Opt. Soc. Am. B **12**, 1602 (1995).

[10] N. V. Kukhtarev, V. Markov, and S. G. Odulov, Opt. Commun. **23**, 338 (1977).

[11] P. Yeh, *Introduction to Photorefractive Nonlinear Optics* (Wiley, New York, 1993), p. 89.

[12] G. K. Harkness, W. J. Firth, J. B. Geddes, J. V. Moloney, and E. M. Wright, Phys. Rev. A **50**, 4310 (1994).

[13] W. Krolikowski, M. R. Belić, M. Cronin-Golomb, and A. Bledowski, J. Opt. Soc. Am. B **7**, 1204 (1990).

[14] B. I. Shraiman, A. Pumir, W. van Saarloos, P. C. Hohenberg, H. Chaté, and M. Holen, Physica D **57**, 241 (1992).

[15] P. Coullet, C. Elphick, L. Gil, and J. Lega, Phys. Rev. Lett. **59**, 884 (1987); P. Coullet and J. Lega, Europhys. Lett. **7**, 511 (1988).

[16] P. C. Hohenberg and B. I. Shraiman, Physica D **37**, 109 (1989).

[17] M. C. Cross and P. C. Hohenberg, Rev. Mod. Phys. **65**, 851 (1993).

[18] R. Vautard and M. Ghil, Physica D **35**, 395 (1989); S. Ciliberto and B. Nicolaenko, Europhys. Lett. **14**, 303 (1991).

[19] O. Hess and E. Schöll, Phys. Rev. A **50**, 787 (1994); O. Hess, Chaos, Solitons & Fractals **4**, 1597 (1994).

[20] H. Lin, J. L. Radloff, and Jianhua Dai, Opt. Commun. **105**, 347 (1994).

[21] M. Brambilla, F. Battipede, L. A. Lugiato, V. Penna, F. Prati, C. Tamm, and C. O. Weiss, Phys. Rev. A **43**, 5090 (1991); K. Staliunas and C. O. Weiss, Physica D **81**, 79 (1995).